Solid State Ionics 251 (2013) 28–33

Contents lists available at ScienceDirect

Solid State Ionics

journal homepage: www.elsevier.com/locate/ssi

Functional properties of SOFC anode materials based on $LaCrO_3$, $La(Ti,Mn)O_3$ and $Sr(Nb,Mn)O_3$ perovskites: A comparative analysis

V.A. Kolotygin [a], E.V. Tsipis [a,b], M.F. Lü [a,c], Y.V. Pivak [a], S.N. Yarmolenko [d], S.I. Bredikhin [e], V.V. Kharton [a,*]

[a] Department of Materials and Ceramic Engineering, CICECO, University of Aveiro, 3810-193 Aveiro, Portugal
[b] UCQR, IST/ITN, Instituto Superior Técnico, Universidade Técnica de Lisboa, CFMC-UL, Estrada Nacional 10, 2686-953 Sacavém, Portugal
[c] State Key Laboratory of Rare Earth Resource Utilization, Changchun Institute of Applied Chemistry CAS, Changchun 130022, PR China
[d] North Carolina A&T State University, Fort IRC Bldg., Suite 242, Greensboro, NC 27411, USA
[e] Institute of Solid State Physics RAS, Institutskaya 2, 142432 Chernogolovka, Moscow region, Russia

ARTICLE INFO

Article history:
Received 13 September 2012
Received in revised form 16 November 2012
Accepted 14 January 2013
Available online 8 February 2013

Keywords:
Oxide anode
Intermediate-temperature SOFCs
Electrode polarization
Electronic conductivity
Chemical expansion
Controlled-atmosphere dilatometry

ABSTRACT

The electrochemical, transport and thermomechanical properties of perovskite-type $(La_{1-x}Sr_x)_{1-y}Mn_{0.5}Ti_{0.5}O_{3-\delta}$ (x = 0.15–0.75; y = 0–0.05), $(La_{0.75-x}Sr_{0.25+x})_{0.95}Mn_{0.5}Cr_{0.5-x}Ti_xO_{3-\delta}$ (x = 0–0.5), $(La_{0.75}Sr_{0.25})_{0.95}Cr_{1-x}Fe_xO_{3-\delta}$ (x = 0.3–0.4), $SrNb_{1-x}Mn_xO_{3-\delta}$ (x = 0.5–0.8) and $(La_{0.9}Sr_{0.1})_{0.95}Cr_{0.85}Mg_{0.1}Ni_{0.05}O_{3-\delta}$ have been appraised in light of their applicability for solid oxide fuel cell (SOFC) anodes. The electrical conductivity, measured in the oxygen partial pressure range of 10^{-20} to 0.5 atm at 940–1270 K, increases with manganese and strontium additions which lead, however, to higher reducibility. In addition to the thermodynamic stability limitations under the SOFC anodic conditions, the latter factor raises the importance of chemically induced expansion, as for Fe-substituted (La,Sr)$CrO_{3-\delta}$. The reduction of Ni-doped chromite results in the formation of nanosized metallic particles dispersed on the perovskite surface, and has no significant effect on the transport properties governed by the perovskite phase. The maximum electrochemical performance was observed for porous $La_{0.5}Sr_{0.5}Mn_{0.5}Ti_{0.5}O_{3-\delta}$, $(La_{0.9}Sr_{0.1})_{0.95}Cr_{0.85}Mg_{0.1}Ni_{0.05}O_{3-\delta}$ and $(La_{0.75}Sr_{0.25})_{0.95}Cr_{0.7}Fe_{0.3}O_{3-\delta}$ electrodes in the electrochemical cells with lanthanum gallate-based solid electrolyte and $Ce_{0.8}Gd_{0.2}O_{2-\delta}$ interlayers.

1. Introduction

Utilization of hydrocarbon-containing fuels in solid oxide fuel cells (SOFCs) makes it necessary to develop novel high-performance anode materials with an improved durability. In general, these materials should satisfy severe requirements, including a high electrochemical and catalytic activity, chemical and microstructural stability under the SOFC operation and fabrication conditions, high electronic and ionic conductivity, compatibility with solid electrolytes, and low cost [1–3]. The conventional Ni-containing cermets exhibit important disadvantages, primarily degradation in hydrocarbon- or sulfur-containing atmospheres and sintering during operation [1–4]. As substituting Ni with other metals does not allow to avoid these problems and/or leads to high costs [2–4], numerous studies were focused on the search of alternative oxide materials, in particular with ABO_3 perovskite structures (e.g. [2,3,5–13]). Quite promising results were reported for chromite- and titanate-based perovskite compositions, since their tolerance to A- and B-site substitution enables the optimization of anode functional properties [5–13]. Extensive doping is necessary for all candidate parent compounds known up to now. For example, chromites are thermodynamically stable under the SOFC anodic conditions and possess moderate thermal and chemical expansion, but suffer from the electronic conductivity drop in reducing atmospheres and a poor electrochemical activity [5–9,12]. Moreover, the presence of chromium is associated with the formation of Cr^{6+} under ambient conditions and volatilization of Cr-containing species [12], and should be minimized. An enhanced electrocatalytic activity and relatively high electronic conduction are characteristic of $(La,Sr)(Cr,Mn)O_{3-\delta}$ and other Mn-containing perovskites where the B-site substituents may shift the onset of phase decomposition and/or conductivity drop to lower oxygen chemical potentials [6,11,14]. Another doping strategy relates to dissolving reducible components (e.g., Ni or Ru) in the perovskite structure and subsequent segregation of metallic particles at low $p(O_2)$ [9,12]; this improves catalytic behavior and transport, but may induce time degradation as for the conventional cermets. Perovskite-like titanates and their derivatives exhibit a high n-type electronic conductivity in reducing conditions; however, their functional properties are strongly susceptible to oxidation, whilst the redox kinetics is often too slow [10,11,13].

The present work is centered on the comparative assessment of several groups of the perovskite-based anode materials, including $(La_{1-x}Sr_x)_{1-y}Mn_{0.5}Ti_{0.5}O_{3-\delta}$ (x = 0.15–0.75; y = 0–0.05), $(La_{0.75-x}Sr_{0.25+x})_{0.95}Mn_{0.5}Cr_{0.5-x}Ti_xO_{3-\delta}$ (x = 0–0.5), $(La_{0.75}Sr_{0.25})_{0.95}Cr_{1-x}Fe_xO_{3-\delta}$ (x = 0.3–0.4), $SrNb_{1-x}Mn_xO_{3-\delta}$ (x = 0.5–0.8) and $(La_{0.9}Sr_{0.1})_{0.95}Cr_{0.85}Mg_{0.1}Ni_{0.05}O_{3-\delta}$. The materials of the three first

* Corresponding author. Tel.: +351 234 370263; fax: +351 234 425300.
E-mail address: kharton@ua.pt (V.V. Kharton).

0167-2738/$ – see front matter © 2013 Elsevier B.V. All rights reserved.
http://dx.doi.org/10.1016/j.ssi.2013.01.005

systems were characterized elsewhere [7,15–17]; in this work their functional properties are compared to one another in order to select promising directions of the oxide electrode developments. In the case of $(La_{0.9}Sr_{0.1})_{0.95}Cr_{0.85}Mg_{0.1}Ni_{0.05}O_{3-\delta}$, the A-site cation deficiency and reduction of Ni under anodic conditions are expected to promote the formation of highly dispersed metallic particles stabilized on the perovskite oxide surface. For other perovskites the target state is single-phase, although the significant concentrations of manganese or iron may lead to partial decomposition in reducing atmospheres. In addition to the phase stability and anode performance, attention was focused on thermomechanical behavior and electronic transport as functions of the oxygen partial pressure and cation composition.

2. Experimental

Fine powders of the oxide materials used for fabrication of porous electrodes and dense ceramics were synthesized by the glycine-nitrate or solid-state reaction routes with subsequent ball-milling. Their characterization included X-ray diffraction (XRD), scanning and transmission electron microscopy (SEM/TEM) coupled with energy-dispersive spectroscopy (EDS), inductively coupled plasma (ICP) spectroscopic analysis, and thermogravimetric analysis (TGA); sintered ceramic samples with >91% density were used for the determination of total electrical conductivity (4-probe DC) as function of the oxygen partial pressure, and controlled-atmosphere dilatometry. The crystal structure was refined by the full-profile Rietveld method using room-temperature XRD patterns. For the analysis of anodic behavior, the electrochemical impedance spectroscopy and overpotential–current density measurements in wet 10% H_2–90% N_2 gas mixture flow were employed using three-electrode cells with $(La_{0.9}Sr_{0.1})_{0.98}Ga_{0.8}Mg_{0.02}O_{3-\delta}$ (LSGM) and $La_{10}Si_5AlO_{26.5}$ solid electrolytes, porous $Ce_{0.8}Gd_{0.2}O_{2-\delta}$ (CGO) interlayer between the working electrode (WE) and electrolyte membrane, porous Pt reference and counter electrodes, and Pt gauze current collectors. Typical WE microstructures are illustrated in Fig. 1(A–C). The experimental techniques and equipment were described in previous works (see [6,7,15–21] and references cited).

3. Results and discussion

XRD analysis confirmed the formation of single perovskite phases in the systems $(La,Sr)(Mn,Cr,Ti)O_{3-\delta}$, $(La,Sr)(Mn,Ti)O_{3-\delta}$ and $(La,Sr)(Cr,Fe)O_{3-\delta}$ under oxidizing conditions. No decomposition was also revealed on their reduction in H_2-containing atmospheres, except for the segregation of trace amounts of MnO observed for several La- and Ti-rich compositions (Fig. 2). The incorporation of iron and increasing Sr^{2+} concentration in these perovskites promotes the transition from rhombohedral (space group $R\bar{3}c$) into orthorhombic (*Pbnm*) polymorph at low oxygen pressures due to higher oxygen deficiency and resultant increase of the B-site cation radii. Phase relationships in the $SrNb_{1-x}Mn_xO_{3-\delta}$ system are more complex. After annealing under reducing conditions, single-phase perovskite with a cubic structure (S.G. $Pm\bar{3}m$) was only found to form at x = 0.5; $SrNb_{0.4}Mn_{0.6}O_{3-\delta}$ forms a mixture of rhombohedral ($R\bar{3}c$) and orthorhombic (*Pnma*) phases with minor MnO impurity alike to manganites–titanates, whereas $SrNb_{0.2}Mn_{0.8}O_{3-\delta}$ tends to entirely decompose. Nevertheless, taking into account the higher electronic conductivity of $SrNb_{0.4}Mn_{0.6}O_{3-\delta}$ (Fig. 3), the latter Nb:Mn concentration ratio seems preferable for the SOFC anode applications in this system. Finally, nickel additive was found to segregate from A-site cation deficient $(La_{0.9}Sr_{0.1})_{0.95}Cr_{0.85}Mg_{0.1}Ni_{0.05}O_{3-\delta}$ regardless of the oxygen chemical

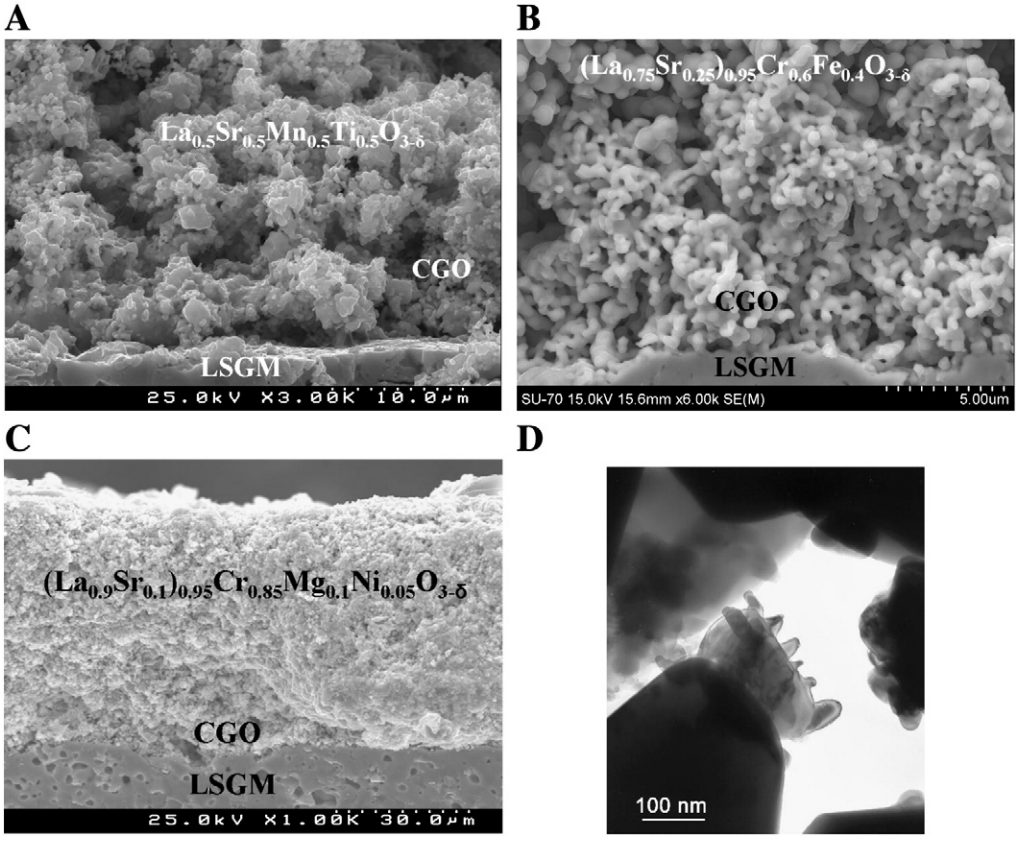

Fig. 1. SEM micrographs of fractured porous $La_{0.5}Sr_{0.5}Mn_{0.5}Ti_{0.5}O_{3-\delta}$ (A), $(La_{0.75}Sr_{0.25})_{0.95}Cr_{0.6}Fe_{0.4}O_{3-\delta}$ (B) and $(La_{0.9}Sr_{0.1})_{0.95}Cr_{0.85}Mg_{0.1}Ni_{0.05}O_{3-\delta}$ (C) electrodes in contact with CGO|LSGM, and TEM image of reduced $(La_{0.9}Sr_{0.1})_{0.95}Cr_{0.85}Mg_{0.1}Ni_{0.05}O_{3-\delta}$ after annealing in H_2-atmosphere at 1173 K (D).

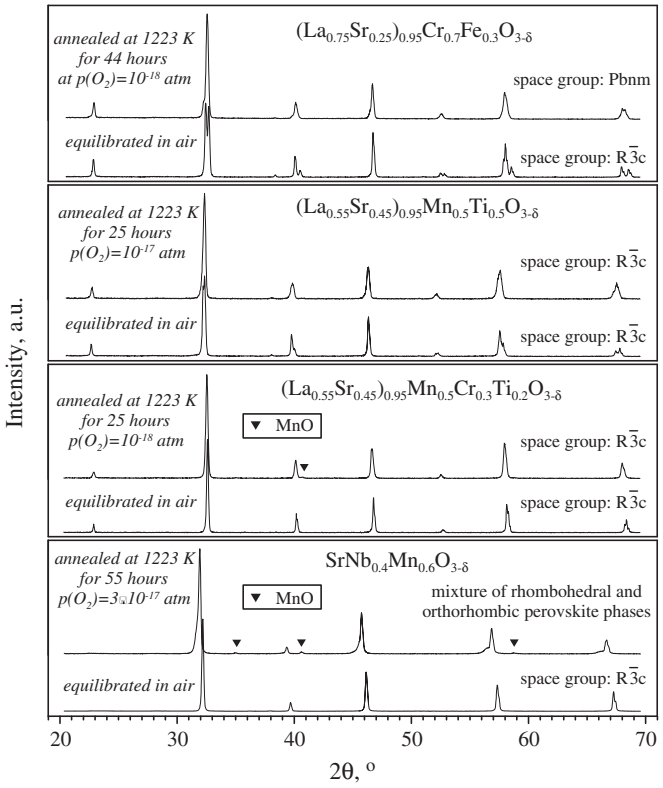

Fig. 2. Selected XRD patterns of the oxide anode materials after equilibration in atmospheric air and after reduction. The annealing conditions in reducing atmospheres are given in the legends. The samples equilibrated at atmospheric oxygen pressure were annealed at 1270–1320 K during 8–15 h and then slowly cooled in air.

potential, forming (Ni,Mg)O solid solution in air and nanosized metallic particles spread over submicron perovskite grains in hydrogen-containing atmospheres (Fig. 1D). This type of morphology is beneficial

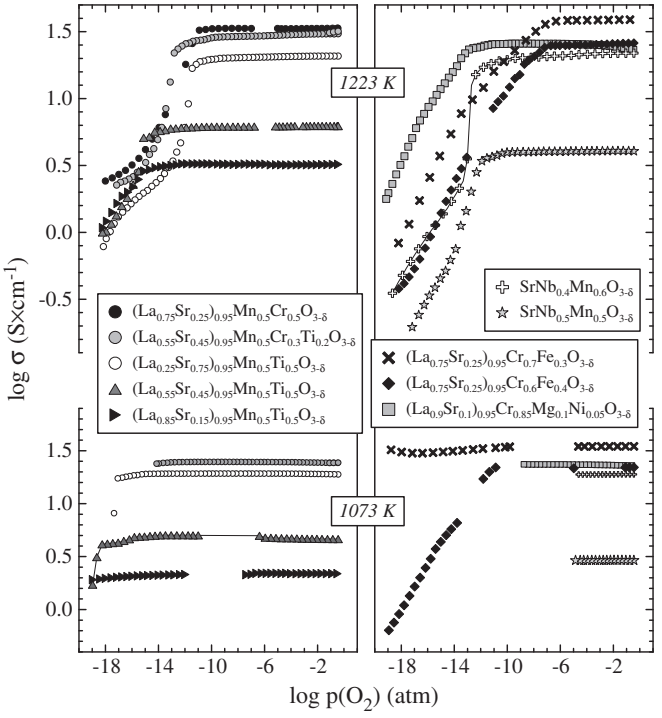

Fig. 3. Oxygen partial pressure dependencies of the total conductivity at 1223 K (top) and 1073 K (bottom). Solid lines are a guide for the eye.

for the catalytic performance, although possible agglomeration of Ni during anode operation may result in a gradual degradation [9].

The oxygen partial pressure dependencies of the total conductivity (Fig. 3) display similar trends for all studied materials. Namely, plateau-like behavior is observed under oxidizing conditions when the oxygen content is close to stoichiometric and essentially constant. In moderately reducing atmospheres, the conductivity (σ) starts to decrease with decreasing $p(O_2)$, indicating that the electronic charge carriers are p-type. Notice that the data on oxygen permeability and Faradaic efficiency [7,15–17] showed that the oxygen ion transference numbers are very low, $<10^{-6}$; the ionic contribution to the total conductivity can hence be neglected. The range of the oxygen partial pressures where σ values are essentially $p(O_2)$-independent, expands on decreasing temperature as the oxygen nonstoichiometry variations decrease. In some cases, the conductivity at 1073 K is almost constant down to $p(O_2) = 10^{-20}$ atm, though this behavior in the intermediate-temperature range may partly originate from kinetic factors. When considering the major effects of cation composition, it should first be mentioned that the incorporation of B-site cations with a relatively stable oxidation state, such as Ti or Nb, decreases hole mobility and conductivity. Consequently, their concentration in the B-sublattice should not be higher than 40–60%. An opposite tendency is observed on increasing the concentration of acceptor-type Sr^{2+} in $(La,Sr)(Mn,Ti)O_{3-\delta}$. The substitution of Sr^{2+} for La^{3+} promotes also delocalization of the electronic charge carriers; for example, increasing x in the $(La_{0.75-x}Sr_{0.25+x})_{0.95}Mn_{0.5}Cr_{0.5-x}Ti_xO_{3-\delta}$ series should not substantially influence the hole concentration due to the electroneutrality condition, but leads to lower activation energy for the p-type electronic transport, E_a (Fig. 4A). On the other hand, Sr^{2+} doping increases reducibility, which is reflected by shifting the onset of the conductivity decrease at low $p(O_2)$. The segregation of metallic nickel in reduced $(La_{0.9}Sr_{0.1})_{0.95}Cr_{0.85}Mg_{0.1}Ni_{0.05}O_{3-\delta}$ has no substantial effect on the transport properties as Ni content is small; the total conductivity of this material in reducing atmospheres is comparable to that of $(La_{0.75}Sr_{0.25})_{0.95}Cr_{0.5}Mn_{0.5}O_{3-\delta}$ and $(La_{0.55}Sr_{0.45})_{0.95}Ti_{0.5}Mn_{0.5}O_{3-\delta}$.

Fig. 4B presents the average thermal expansion coefficients (TECs) calculated from the dilatometric data in air and in reducing atmosphere. For most studied materials the TECs at 923–1223 K vary in the range $(11–14)\times10^{-6}$ K^{-1} and are compatible with those of solid oxide electrolytes, such as $(La_{0.9}Sr_{0.1})_{0.98}Ga_{0.8}Mg_{0.2}O_{3-\delta}$ (LSGM) and $La_{10}Si_5AlO_{26.5}$ [18,19]. Increasing strontium and manganese concentrations in the perovskite lattice yields a moderately higher thermal expansion, in correlation with reducibility reflected by the conductivity vs. $p(O_2)$ variations. Whatever the relevant mechanisms under oxidizing conditions when the oxygen nonstoichiometry is low, an increase in apparent TECs in reducing atmospheres is associated with the chemical expansion, primarily caused by increasing B-site cation radii on reduction (Fig. 5A). The isothermal chemical strains (Fig. 5B) are maximum for the $(La,Sr)(Cr,Fe)O_{3-\delta}$ system; the perovskite manganites–titanates exhibit a considerably better dimensional stability, although their chemical expansivity tends to increase with Sr^{2+} additions. At the same time, redox cycling of dense $(La,Sr)(Mn,Ti)O_{3-\delta}$ ceramics with large La^{3+} content leads often to cracking. Compared to other compositions, the best thermomechanical properties in the studied oxide systems are characteristic of $(La,Sr)Mn_{0.5}Ti_{0.5}O_{3-\delta}$ where the La:Sr cation concentration ratio is close to unity.

Typical anodic polarization curves of the porous oxide electrodes in wet 10% H_2–90% N_2 atmosphere are shown in Fig. 6; Fig. 7 presents the data on polarization resistance at 1073 K. In general, the overpotentials of similar electrodes in contact with LSGM are significantly lower than those for apatite-type $La_{10}Si_5AlO_{26.5}$ (Fig. 6A) owing to the higher ionic and electronic conductivities of lanthanum gallate and to a relatively poor stability of silicate-based solid electrolytes, resulting in silica segregation and spreading on the electrode/electrolyte interface and electrode surface [18,19,21]. For both electrolytes, the anode performance is substantially improved by introducing the protective CGO sublayers, which enlarge the electrochemical reaction zone

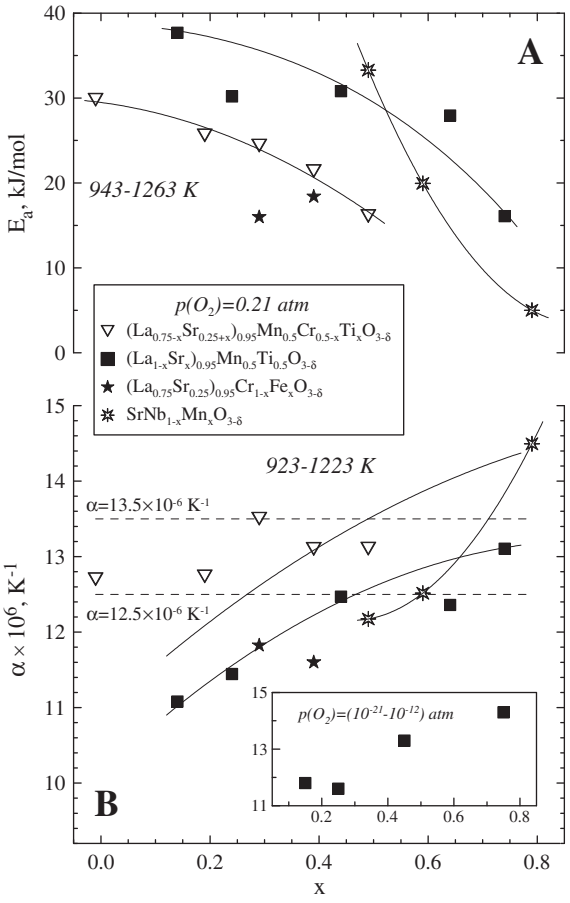

Fig. 4. Composition dependencies of the activation energy for total conductivity (A) and average TECs (B) in air. Inset shows the average TECs of $(La_{1-x}Sr_x)_{1-y}Mn_{0.5}Ti_{0.5}O_{3-\delta}$ perovskites in CO–CO_2 atmosphere.

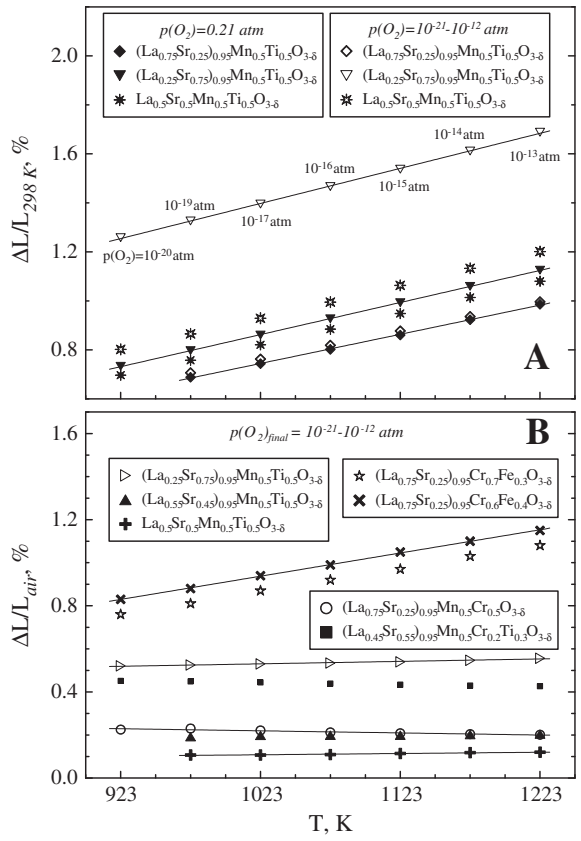

Fig. 5. Thermal expansion measured in the regime of temperature cycling with 2–5 h dwells at each temperature in air and under reducing conditions (A), and isothermal chemically-induced strain relative to the atmospheric oxygen pressure (B). $L_{298\ K}$ is the room-temperature length. $\Delta L/L_{air}$ is the relative elongation on isothermal equilibration in CO–CO_2 atmospheres, normalized to the length at the same temperature and atmospheric oxygen pressure; the temperature-dependent $p(O_2)$ values in CO–CO_2 gas mixture are given in (A). Solid lines are a guide for the eye.

and suppress cation interdiffusion between the electrode and electrolyte membranes, as confirmed by EDS analysis. The maximum electrochemical activity in the studied series was observed for several electrode materials with essentially different cation compositions, in particular $(La_{0.75}Sr_{0.25})_{0.95}Cr_{0.7}Fe_{0.3}O_{3-\delta}$, $La_{0.5}Sr_{0.5}Mn_{0.5}Ti_{0.5}O_{3-\delta}$ and $(La_{0.9}Sr_{0.1})_{0.95}Cr_{0.85}Mg_{0.1}Ni_{0.05}O_{3-\delta}$. Their overpotentials are quite similar to one another, but are still higher compared to Ni-containing cermet (Fig. 6B).

Previous studies [7,15] showed that the anode performance can be substantially increased by infiltration of $CeO_{2-\delta}$ or Ni; one example supporting this conclusion is presented in Fig. 6A. Such an enhancement cannot be ascribed to any single mechanism, since the infiltration leads to a larger electrode surface area, to the deposition of nanosized particles with high catalytic activity onto the electrolyte surface and in the vicinity of triple-phase boundary, to improved intergranular contacts in the porous electrode layers, and to an increased electronic conductivity of the anodes. The relevance of the former factors is confirmed by the fact that, although the conductivity of reduced $CeO_{2-\delta}$ is comparable to that of the perovskite phases, ceria infiltration provides 2–3 times lower overpotentials (Fig. 6A). Nonetheless, in combination with significant effects of the current collector geometry [7] and the conductivity decrease under reducing conditions (Fig. 3), this behavior indicates that the electronic transport is one of the performance-limiting factors. The same conclusion can be drawn from the correlation between the polarization resistance and conductivity (Fig. 7). Note, however, that the empirical correlation presented in Fig. 7 is not ideal, indicating that other polarization-affecting factors cannot be ignored as well. These include, at least, electrode microstructure, the presence of electrochemically active species on the anode surface, metal–oxygen bond strength and surface concentration of oxygen vacancies determining the electrochemical behavior of the perovskite phases. The latter seems partly responsible for the high electrochemical activity of $(La,Sr)(Cr,Fe)O_{3-\delta}$ having rather modest electronic conductivity (Fig. 7), but increases chemical expansion of these perovskites (Fig. 5B). These properties of $(La,Sr)(Cr,Fe)O_{3-\delta}$ perovskites all correlate with a lower average charge of the B-site cations if compared to the Nb- and Ti-containing phases, thus providing weaker metal–oxygen bonding.

Finally, the optimization of anode materials makes it necessary to take into account their thermodynamic and kinetic stability under ambient conditions and during startup/shutdown. All compositions studied in the present work exhibit non-negligible surface hydration and chromium oxidation by atmospheric oxygen at low temperatures, in agreement with literature [12]. Fig. 8 illustrates typical weight losses and hysteresis phenomena originating from the water vapor and oxygen desorption on heating, studied by TGA for the powders with similar thermal prehistory; after the synthesis, all the materials were slowly cooled down to room temperature in atmospheric air and then kept in dried air atmosphere during approximately 30–40 days. Due to the differences in the powder morphology and cation composition affecting the reaction mechanisms, quantitative analysis of the TGA data is impossible. However, these results clearly indicate that the tendencies to surface oxidation and hydration become more pronounced when the content of Cr and Sr cations increases. Large concentrations of chromium seem

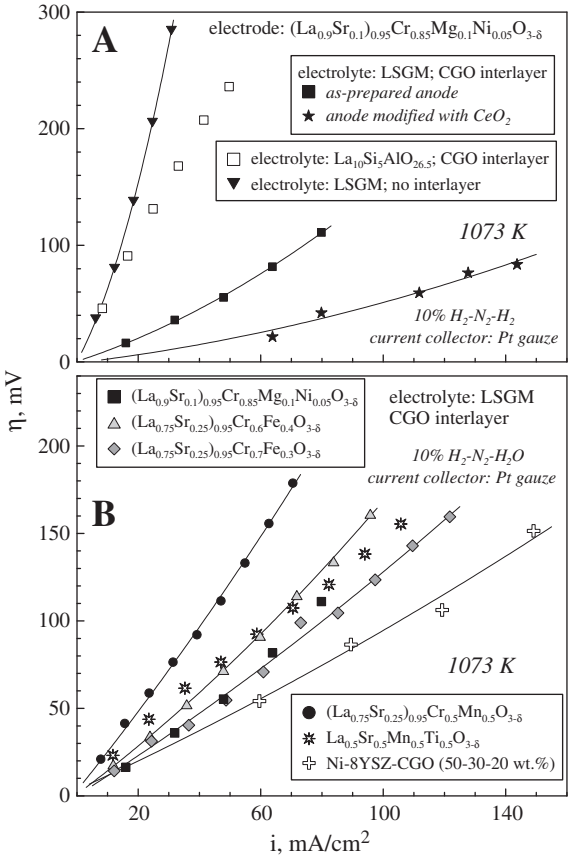

Fig. 6. Anodic overpotential vs. current density dependencies for various half-cells with porous $(La_{0.9}Sr_{0.1})_{0.95}Cr_{0.85}Mg_{0.1}Ni_{0.05}O_{3-\delta}$ anode layer (A), and comparison of oxide anodes deposited onto LSGM solid electrode with CGO interlayer (B), at 1073 K. The data on the cermet anode containing metallic Ni, 8 mol% yttria-stabilized zirconia (8YSZ) and CGO [20] are shown for comparison.

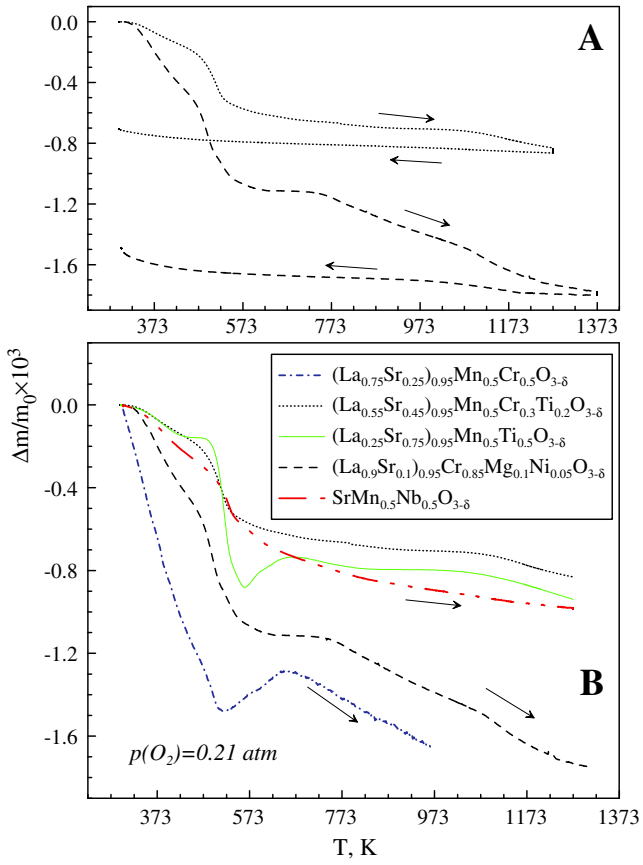

Fig. 8. Comparison of the relative weight changes of the oxide electrode materials, measured by TGA in dried atmospheric air. Arrows show the direction of the temperature changes. The top part (A) illustrates typical hestereses observed on heating and subsequent cooling.

to play a more negative role; for example, the maximum weight losses at 300–700 K were observed for $(La_{0.9}Sr_{0.1})_{0.95}Cr_{0.85}Mg_{0.1}Ni_{0.05}O_{3-\delta}$ and $(La_{0.75}Sr_{0.25})_{0.95}Mn_{0.5}Cr_{0.5}O_{3-\delta}$. Moreover, it should be mentioned that these losses may be contributed by volatilization of Cr-containing species, such as CrO_3. Comparison of the stability and electrochemical, electrical and thermomechanical behavior shows, therefore, that the most appropriate combination of the anode functional properties is observed for $(La_{0.5}Sr_{0.5})_{1-y}Mn_{0.5}Ti_{0.5}O_{3-\delta}$ perovskites and their derivatives; further

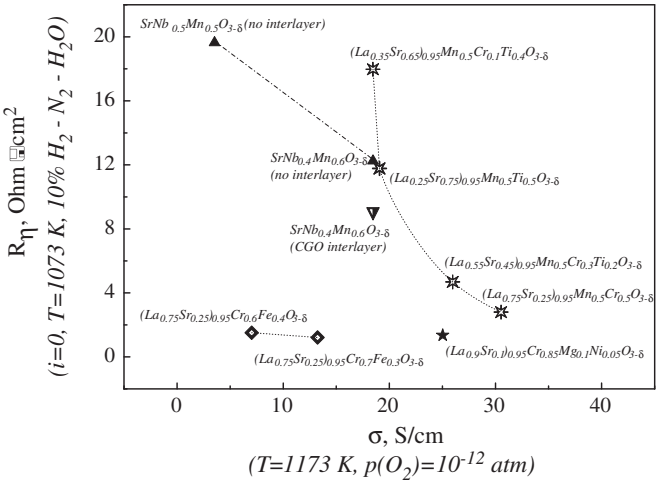

Fig. 7. Correlation between the anodic polarization resistance and total conductivity of the electrode materials. All dashed lines are a guide for the eye.

improvements can be expected on their surface modification with nickel and ceria appraised for another model composition, $(La_{0.9}Sr_{0.1})_{0.95}Cr_{0.85}Mg_{0.1}Ni_{0.05}O_{3-\delta}$.

Acknowledgements

This work was supported by FCT, Portugal (projects PEst-C/CTM/LA0011/2011, PTDC/CTM-CER/114561/2009, SFRH/BPD/28629/2006 and SFRH/BD/45227/2008), by the Ministry of Education and Science of the Russian Federation (state contracts 02.740.11.5214 and 11.519.11.6002), and by the NSF, USA (project DMR-0502765). Experimental assistance and helpful discussions made by A. Ivanov, A. Yaremchenko and A. Shaula are gratefully acknowledged.

References

[1] B.C.H. Steele, Solid State Ionics 86 (1996) 1223.
[2] J.B. Goodenough, Y.H. Huang, J. Power. Sources 173 (2007) 1.
[3] E.V. Tsipis, V.V. Kharton, J. Solid State Electrochem. 12 (2008) 1367.
[4] R.J. Gorte, J.M. Vohs, S. McIntosh, Solid State Ionics 175 (2004) 1.
[5] S. Primdahl, J.R. Hansen, L. Grahl-Madsen, P.H. Larsen, J. Electrochem. Soc. 148 (2001) A74.
[6] S. Tao, J.T.S. Irvine, J. Electrochem. Soc. 151 (2004) A252.
[7] V.V. Kharton, E.V. Tsipis, I.P. Marozau, A.P. Viskup, J.R. Frade, J.T.S. Irvine, Solid State Ionics 178 (2007) 101.
[8] S. McIntosh, M. van den Bossche, Solid State Ionics 192 (2011) 453.
[9] B.D. Madsen, W. Kobsiriphat, Y. Wang, L.D. Marks, S.A. Barnett, J. Power. Sources 166 (2007) 64.
[10] O.A. Marina, N.L. Canfield, J.W. Stevenson, Solid State Ionics 149 (2002) 21.
[11] Q.X. Fu, F. Tietz, D. Stoever, J. Electrochem. Soc. 153 (2006) D74.
[12] J. Sfeir, J. Power. Sources 118 (2003) 276.
[13] S. Hui, A. Petric, Mater. Res. Bull 37 (2002) 1215.

[14] S. Tao, J.T.S. Irvine, J. Mater. Chem. 12 (2002) 2356.
[15] V.A. Kolotygin, E.V. Tsipis, A.L. Shaula, E.N. Naumovich, J.R. Frade, S.I. Bredikhin, V.V. Kharton, J. Solid State Electrochem. 15 (3) (2011) 13.
[16] V.A. Kolotygin, E.V. Tsipis, A.I. Ivanov, Y.A. Fedotov, I.N. Burmistrov, D.A. Agarkov, V.V. Sinitsyn, S.I. Bredikhin, V.V. Kharton, J. Solid State Electrochem. 16 (2012) 2335.
[17] M.F. Lu, E.V. Tsipis, J.C. Waerenborgh, A.A. Yaremchenko, V.A. Kolotygin, S. Bredikhin, V.V. Kharton, J. Power. Sources 206 (2012) 59.
[18] A.L. Shaula, V.V. Kharton, F.M.B. Marques, J. Solid State Chem. 178 (2005) 2050.
[19] V.V. Kharton, A.L. Shaula, N.P. Vyshatko, F.M.B. Marques, Electrochim. Acta 48 (2003) 1817.
[20] E.V. Tsipis, V.V. Kharton, I.A. Bashmakov, E.N. Naumovich, J.R. Frade, J. Solid State Electrochem. 8 (2004) 674.
[21] E.V. Tsipis, V.V. Kharton, J.R. Frade, Electrochim. Acta 52 (2007) 4428.